NASA TECHNICAL NOTE

NASA TN D-4360

NASA TN D-4360

COMPARISON OF THE MACH 3.0 AERODYNAMIC CHARACTERISTICS OF TENSION STRING, TENSION SHELL, AND 120° CONICAL SHAPES

by James Wayne Sawyer
Langley Research Center
Langley Station, Hampton, Va.

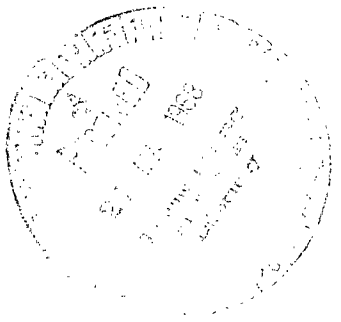

NATIONAL AERONAUTICS AND SPACE ADMINISTRATION • WASHINGTON, D. C. • MARCH 1968

COMPARISON OF THE MACH 3.0 AERODYNAMIC CHARACTERISTICS OF TENSION STRING, TENSION SHELL, AND 120° CONICAL SHAPES

By James Wayne Sawyer

Langley Research Center
Langley Station, Hampton, Va.

NATIONAL AERONAUTICS AND SPACE ADMINISTRATION

For sale by the Clearinghouse for Federal Scientific and Technical Information
Springfield, Virginia 22151 – CFSTI price $3.00

COMPARISON OF THE MACH 3.0 AERODYNAMIC CHARACTERISTICS OF TENSION STRING, TENSION SHELL, AND 120° CONICAL SHAPES

By James Wayne Sawyer
Langley Research Center

SUMMARY

An investigation was conducted at a Mach number of 3.0 to determine aerodynamic characteristics of three decelerator shapes based on the tension string structural concept. The shapes were tested at angles of attack up to 12° and at free-stream Reynolds numbers, based on maximum body diameter, of approximately 1.0×10^6 and 3.0×10^6. A comparison was made between the aerodynamic characteristics thus obtained and published results for a 120° cone and comparable tension shell configurations. The results showed that the tension string shapes were more susceptible to flow separation than the tension shell shapes, but the aerodynamic coefficients of the tension string shapes were not affected by the onset of flow separation as much as were the aerodynamic characteristics of the tension shell shapes. The aerodynamic coefficients, static stability, and aerodynamic centers of the tension string shapes showed little sensitivity to variation in body length and nose radius and, in general, approximated those of the cone.

INTRODUCTION

Considerable effort has been directed toward developing high-drag shapes that are aerodynamically stable for use with low-mass structures in applications requiring aerodynamic deceleration within low-density atmospheres. Although several promising concepts have emerged from this effort, none completely satisfies all the requirements. For example, among the shapes that have received attention are the large-angle cone and those based on the tension shell concept of reference 1 (see refs. 2 to 9). The large-angle cone has shown relatively high drag coefficients and acceptable static stability characteristics, but structurally it is not very efficient. On the other hand, shapes based on the more structurally efficient tension shell structure have shown drag coefficients that were substantially higher than those for a 120° cone, but also showed less favorable static stability characteristics.

Recently another structural concept, called the tension string structure, was advanced in reference 10 for use in similar applications. The aerodynamic-load-carrying surface is a truncated hyperboloid of revolution generated by closely spaced taut strings

wound over two compression rings. Inasmuch as data on the aerodynamic characteristics of shapes based on the concept were unavailable, the present investigation was undertaken to provide measurements of the aerodynamic forces and moments of three tension string shapes.

The investigation was conducted in the Langley 9- by 6-inch model tunnel at a Mach number of 3.0, angles of attack up to 12^{o}, and Reynolds numbers, based on maximum model diameter, of approximately 1.0×10^{6} and 3.0×10^{6}. The data obtained were then compared with data reported in reference 2 for a 120^{o} cone and four tension shell shapes having proportions similar to those of the tension string shapes. The results are presented herein.

SYMBOLS

The units used for the physical quantities in this paper are given both in the U.S. Customary Units and in the International System of Units (SI). Factors relating the two systems are given in reference 11, and those used in the present investigation are presented in the appendix.

A^2 shape parameter associated with Newtonian pressure (see ref. 1)

A_b projected base area, πr_{max}^2

C_A axial-force coefficient, $\frac{\text{Axial force}}{qA_b}$

C_N normal-force coefficient, $\frac{\text{Normal force}}{qA_b}$

C_m pitching-moment coefficient, $\frac{\text{Pitching moment}}{2qA_b r_{max}}$

C_{m_α} slope of pitching-moment curve at zero angle of attack, $\left(\frac{\partial C_m}{\partial \alpha}\right)_{\alpha=0^o}$

C_{N_α} slope of normal-force curve at zero angle of attack, $\left(\frac{\partial C_N}{\partial \alpha}\right)_{\alpha=0^o}$

l model forebody length (fig. 1)

M free-stream Mach number

q dynamic pressure

R Reynolds number based on maximum model diameter

r	radial coordinate
r_{max}	maximum model radius
r_n	spherical nose radius
x	axial coordinate (fig. 1)
x_{ac}	axial coordinate of aerodynamic center, $\frac{C_{m_\alpha}}{C_{N_\alpha}} + \frac{1}{4}$
α	angle of attack
δ	flow turning angle

MODELS, APPARATUS, AND TESTS

Models

Three tension string shapes were tested in this investigation. The tension string models consisted of a nose cap, a tension-string-shaped forebody, and a conical afterbody, as shown in figure 1(a). The tension string shape is a truncated hyperboloid of revolution generated by closely spaced taut strings wound over two compression rings. Different body configurations are obtained by varying the ring diameters, the distance between rings, and the nose shape. The tension string shapes are designated by numerals in order of increasing forebody length. Model 1 was a spherically blunted $\left(r_n/r_{max} = 0.355\right)$ version of model 2 which had a pointed conical nose cap. Model 3 had a forebody profile that fell slightly below that of models 1 and 2, and its nose cap was a spherically blunted cone. All three tension string shapes were constructed with a corner radius of 0.022 inch (0.056 cm) at the maximum diameter of 1.25 inches (3.10 cm). The models were machined from aluminum alloy and were polished to a finish of approximately 10 microinches (250 nm).

Sketches of the four tension shell shapes selected for comparison with the tension string models are shown in figure 1(b). These shapes are designated by letters in order of increasing length. Models A and C are spherically blunted $\left(r_n/r_{max} = 0.10\right)$ versions of models B and D. The value of the shape parameter A^2 used in deriving the shapes for models A and B was 0.835 and that for models C and D was 1.058 (ref. 1). The tip of the 120^o conical model was pointed $\left(r_n/r_{max} = 0\right)$. Coordinates for the tension-string-shaped and tension-shell-shaped models are presented in table I.

Test Facility

Tests of the tension string shapes were conducted in the Langley 9- by 6-inch model tunnel. This facility is a supersonic (M = 3.0) blowdown wind tunnel with an air storage and pumping capacity sufficient to permit continuous operation of the model tunnel at ambient stagnation temperature. The tunnel stagnation-pressure operating range is from 55 to 200 pounds per square inch absolute $(380 \text{ to } 1380 \text{ kN/m}^2)$ and the stagnation-temperature range is from ambient to 3000° F (1900° K). Calibration tests of the tunnel test section showed a maximum deviation in Mach number of less than 1 percent.

Models are sting mounted to an angle-of-attack mechanism capable of pitching the model through 12°. Angle of attack is determined by recording the output from a linear potentiometer attached to the angle-of-attack mechanism. The angle-of-attack measurements do not take into account sting deflection due to model airloads, but static-load calculations showed that the sting deflection should not exceed 0.3°.

Instrumentation and Tests

Aerodynamic forces and pitching moments were measured with a three-component, strain-gage balance which was externally mounted with respect to the model. A shroud was used to shield the sting-balance assembly from the airstream, and a light was installed to indicate contact between the shroud and sting.

Model base pressure was measured by means of an orifice tube located near the base of the model in the yaw plane. Output from the pressure transducers and strain-gage balance was recorded by the Langley central digital data recording facility.

A single-pass horizontal Z-light-path schlieren system with a horizontal knife edge was used in conjunction with a camera to record the shock waves and flow patterns about the models. The schlieren photographs shown in this report were taken with two different light sources. The schlieren photographs of the tension string models were taken with a spark light source of approximately 0.2-microsecond duration, whereas the photographs from reference 2 were taken with a mercury vapor bulb having a 3-microsecond flash duration.

Estimated maximum experimental errors are as follows:

	$R \approx 1.0 \times 10^6$	$R \approx 3.0 \times 10^6$
C_A	±0.024	±0.008
C_m	±0.010	±0.004
C_N	±0.008	±0.002

All tests were conducted at ambient stagnation temperatures and at stagnation-pressure levels of 60 and 170 pounds per square inch absolute $(410 \text{ and } 1170 \text{ kN/m}^2)$. Corresponding Reynolds numbers, based on model maximum diameter, were approximately 1.0×10^6 and 3.0×10^6. All models were tested at angles of attack from 0° to 12° in 3° increments.

The test procedure was to start the tunnel with the model at zero angle of attack and to maintain a stagnation pressure of 60 pounds per square inch absolute (410 kN/m^2) until the flow conditions reached equilibrium. Data were then recorded for approximately 5 seconds. Next, the stagnation pressure was increased to the high level. After another 5-second data acquisition period, the tunnel stagnation pressure was returned to the low level, and the procedure was repeated for the other angles of attack. No data were acquired during the change from one angle of attack to another.

All experimental axial-force data presented have been corrected to a free-stream static-pressure condition at the model base. Actual measured C_A values were approximately 0.11 higher than shown. The moment center was located at a distance upstream from the maximum body diameter of 50 percent of the base radius.

RESULTS AND DISCUSSION

Flow Patterns

Typical schlieren photographs of flow patterns about all models at $\alpha = 0^\circ$ and 12° are shown in figure 2 for $R \approx 1.0 \times 10^6$ and in figure 3 for $R \approx 3.0 \times 10^6$. The shorter tension string and tension shell models (1, 2, A, and B) generated a detached bow wave similar to that of the 120° cone, whereas the longer models (3, C, and D) showed a double-shock-wave pattern. For models of comparable forebody length, the tension string shapes showed the most susceptibility to flow separation. In table II, the separation events observed from schlieren photographs are summarized for all test values of α and R. The question marks indicate instances in which a separated boundary layer was not clearly defined. In such cases, the schlieren photographs showed a thickening of the boundary layer and thus a tendency toward flow separation. At the low Reynolds number, the tension string shapes (in particular, models 1 and 2) showed the same effect of nose radius as did the tension shell shapes C and D; that is, model 1 – because of its larger nose radius – encountered flow separation on the leeward surface at smaller values of α than did model 2.

Aerodynamic Characteristics

The variations of the pitching-moment, axial-force, and normal-force coefficients with angle of attack are shown in figure 4 for all models at $R \approx 1.0 \times 10^6$ and in figure 5

at $R \approx 3.0 \times 10^6$. The nonzero pitching-moment and normal-force coefficients shown at $\alpha = 0^o$ are attributed primarily to a nonuniform temperature distribution along the strain-gage balance. Additional tests have indicated that the balance sensitivity should not have changed appreciably, and therefore the slopes of the curves should be valid. The data show that the aerodynamic coefficients of the tension string models vary in a manner similar to those of the cone – that is, the C_m and C_N variations are nearly linear; the slopes of the C_m and C_N curves approximate those of the cone, as do the C_A values. Although the tension string shapes encountered flow separation, the linearity of the data suggests that their aerodynamic coefficients were unaffected by the onset of flow separation. The slopes of the C_m and C_N curves for the tension string and the conical shapes are generally greater than those for the tension shell shapes, whereas the slopes of the C_A curves for all models remain nearly constant with α. The values of C_A for the tension shell shapes, however, are between approximately 12 and 18 percent greater than those for the tension string and cone shapes. The difference in C_A values is attributed to the smaller flow turning angle of the tension string shapes and the cone with respect to the tension shell shapes. This observation is supported in reference 3, which shows a decline in C_A as the flow turning angle decreases.

The axial-force coefficients at $\alpha = 0^o$ are compared at both Reynolds numbers in the bar graph of figure 6. Variations in body length and nose radius had little influence on the tension-string and tension-shell C_A values. Increasing the Reynolds number resulted in a drop in the C_A values for all the shapes, but the change in C_A was generally greater for the tension shell shapes.

In figure 7, the parameters C_{m_α} and C_{N_α} and the aerodynamic centers of all the shapes are presented. Although neither the tension-string nor the tension-shell C_{N_α} values appear greatly affected by variations in body length and nose radius, the values of C_{m_α} and the aerodynamic centers of the tension string shapes show less sensitivity to such variations and approximate those of the cone. When the body length is increased, however, a decreasing trend of C_{m_α}, and hence static stability, results, and the aerodynamic centers are shifted upstream. The effect of Reynolds number on C_{m_α} and C_{N_α} appears inconsistent, but with the exception of the cone and the tension shell shape C, an increase in Reynolds number generally caused the aerodynamic center to move downstream. Although all the shapes appear statically stable as shown by the negative C_{m_α} values, the relatively larger negative C_{m_α} values for the tension string and cone models indicate that these shapes are more statically stable than the tension shell shapes. However, two of the tension shell shapes, models A and B, show aerodynamic centers that are farther downstream than any of those of the tension string shapes at the higher Reynolds number.

CONCLUSIONS

Three decelerator shapes based on the tension string structural concept were tested at a Mach number of 3.0 in the Langley 9- by 6-inch model tunnel at angles of attack from 0° to 12° and at Reynolds numbers, based on maximum diameter, of 1.0×10^6 and 3.0×10^6. The schlieren and aerodynamic-coefficient data obtained were compared with previously published data for four tension shell shapes and a 120° cone. The following conclusions were made:

1. For models of approximately the same length, the tension string shapes appeared more susceptible to flow separation at small angles of attack than the tension shell shapes or cone.

2. Although all the tension string shapes encountered flow separation, the force and pitching-moment coefficients appeared unaffected by the onset of flow separation.

3. The aerodynamic coefficients, static stability, and centers of pressure of the tension string shapes showed little sensitivity to variations in body length and nose radius and, in general, approximated those of the 120° cone.

4. The axial-force coefficients for the tension shell shapes were between approximately 12 and 18 percent higher than those for the cone and tension string shapes.

Langley Research Center,
National Aeronautics and Space Administration,
Langley Station, Hampton, Va., August 14, 1967,
124-08-06-03-23.

APPENDIX

CONVERSION OF U.S. CUSTOMARY UNITS TO SI UNITS

The International System of Units (SI) was adopted by the Eleventh General Conference on Weights and Measures held in Paris, October 1960. (See ref. 11.) Factors required for converting the U.S. Customary Units used herein to the International System of Units (SI) are given in the following table:

Physical quantity	U.S. Customary Unit	Conversion factor (*)	SI Unit (**)
Length	in.	0.0254	meters (m)
Pressure	psi	6.895×10^3	newtons/meter^2 (N/m^2)
Temperature . . .	^oF	$\frac{5}{9}(F^o + 460)$	degrees Kelvin (^oK)

*Multiply value given in U.S. Customary Unit by conversion factor to obtain equivalent value in SI Units.

**Prefixes to indicate multiples of units are as follows:

Prefixes	Multiple
centi (c)	10^{-2}
kilo (k)	10^3
nano (n)	10^{-9}

REFERENCES

1. Anderson, Melvin S.; Robinson, James C.; Bush, Harold G.; and Fralich, Robert W.: A Tension Shell Structure for Application to Entry Vehicles. NASA TN D-2675, 1965.

2. Deveikis, William D.; and Sawyer, James Wayne: Aerodynamic Characteristics of Tension Shell Shapes at Mach 3.0. NASA TN D-3633, 1966.

3. Sawyer, James Wayne; and Deveikis, William D.: Effects of Configuration Modifications on Aerodynamic Characteristics of Tension Shell Shapes at Mach 3.0. NASA TN D-4080, 1967.

4. Robinson, James C.; and Jordan, Alfred W.: Exploratory Experimental Aerodynamic Investigation of Tension Shell Shapes at Mach 7. NASA TN D-2994, 1965.

5. Bernot, Peter T.: Longitudinal Stability Characteristics of Several Proposed Planetary Entry Vehicles at Mach 6.73. NASA TN D-2785, 1965.

6. Gibson, Fredrick W.: Aerodynamic Investigation of Some High-Drag Entry Shapes at Mach 15.4. NASA TN D-4134, 1967.

7. Creel, Theodore R., Jr.: Longitudinal Aerodynamic Characteristics of a Tension Shell Entry Configuration at Mach 20. NASA TN D-3541, 1966.

8. Harris, Charles D.: Transonic Aerodynamic Investigation of Tension Shell and Blunted 100^{o} Conical Shapes for Unmanned Entry Vehicles. NASA TN D-3700, 1966.

9. Campbell, James F.: Longitudinal Aerodynamic Characteristics of Several High-Drag Bodies at Mach Numbers from 1.50 to 4.63. NASA TN D-3915, 1967.

10. Alai, John A.: The Tension String Structure. AIAA/ASME Seventh Structures and Materials Conference, Apr. 1966, pp. 447-458.

11. Mechtly, E. A.: The International System of Units – Physical Constants and Conversion Factors. NASA SP-7012, 1964.

TABLE I.- MODEL COORDINATES

r/r_{max}	x/r_{max} for –						
	Tension string			Tension shell			
	Model 1	Model 2	Model 3	Model A	Model B	Model C	Model D
0	[a] $\left(\frac{r_n}{r_{max}} = 0.35\right)$	0.691	[b] $\left(\frac{r_n}{r_{max}} = 0.12\right)$	[c] $\left(\frac{r_n}{r_{max}} = 0.10\right)$	0.600	[d] $\left(\frac{r_n}{r_{max}} = 0.10\right)$	0.800
.05		.649			.554		.737
.10		.607	↓	0.507	.507	0.674	.674
.15		.565	0.599	.462	.462	.612	.612
.20		.523	.529	.417	.417	.551	.551
.25	↓	.481	.463	.373	.373	.492	.492
.30	0.434	.434	.407	.331	.331	.435	.435
.35	.389	.389	.361	.290	.290	.380	.380
.40	.354	.354	.327	.251	.251	.328	.328
.45	.322	.322	.296	.216	.216	.279	.279
.50	.292	.292	.268	.180	.180	.234	.234
.55	.264	.264	.241	.148	.148	.192	.192
.60	.237	.237	.216	.119	.119	.153	.153
.65	.209	.209	.190	.092	.092	.119	.119
.70	.182	.182	.166	.069	.069	.088	.088
.75	.155	.155	.142	.049	.049	.062	.062
.80	.129	.129	.117	.032	.032	.040	.040
.85	.103	.103	.094	.018	.018	.023	.023
.90	.077	.077	.070	.008	.008	.011	.011
.95	.051	.051	.046	.002	.002	.003	.003
1.00	.022	.022	.023	0	0	0	0

[a] Tangent at $\frac{r}{r_{max}} = 0.29$.

[b] Tangent at $\frac{r}{r_{max}} = 0.12$.

[c] Tangent at $\frac{r}{r_{max}} = 0.07$.

[d] Tangent at $\frac{r}{r_{max}} = 0.08$.

TABLE II. – SUMMARY OF FLOW SEPARATION EVENTS

Model	R	Surface	α, deg				
			0	3	6	9	12
1	1.0×10^6	Leeward		?	?	▒	▒
		Windward					
	3.0×10^6	Leeward					?
		Windward					
2	1.0×10^6	Leeward					?
		Windward					
	3.0×10^6	Leeward					▒
		Windward					
3	1.0×10^6	Leeward	▒	▒	▒	▒	▒
		Windward	▒	?			
	3.0×10^6	Leeward	▒	▒	▒	▒	▒
		Windward	▒	?			
120° cone	1.0×10^6	Leeward					
		Windward					
	3.0×10^6	Leeward					
		Windward					
A	1.0×10^6	Leeward					
		Windward					
	3.0×10^6	Leeward					
		Windward					
B	1.0×10^6	Leeward					
		Windward					
	3.0×10^6	Leeward					
		Windward					
C	1.0×10^6	Leeward		▒	▒	▒	▒
		Windward					
	3.0×10^6	Leeward		▒	▒	▒	▒
		Windward					
D	1.0×10^6	Leeward					
		Windward					
	3.0×10^6	Leeward					
		Windward					

▒ Separated flow

? Separated flow not clearly defined

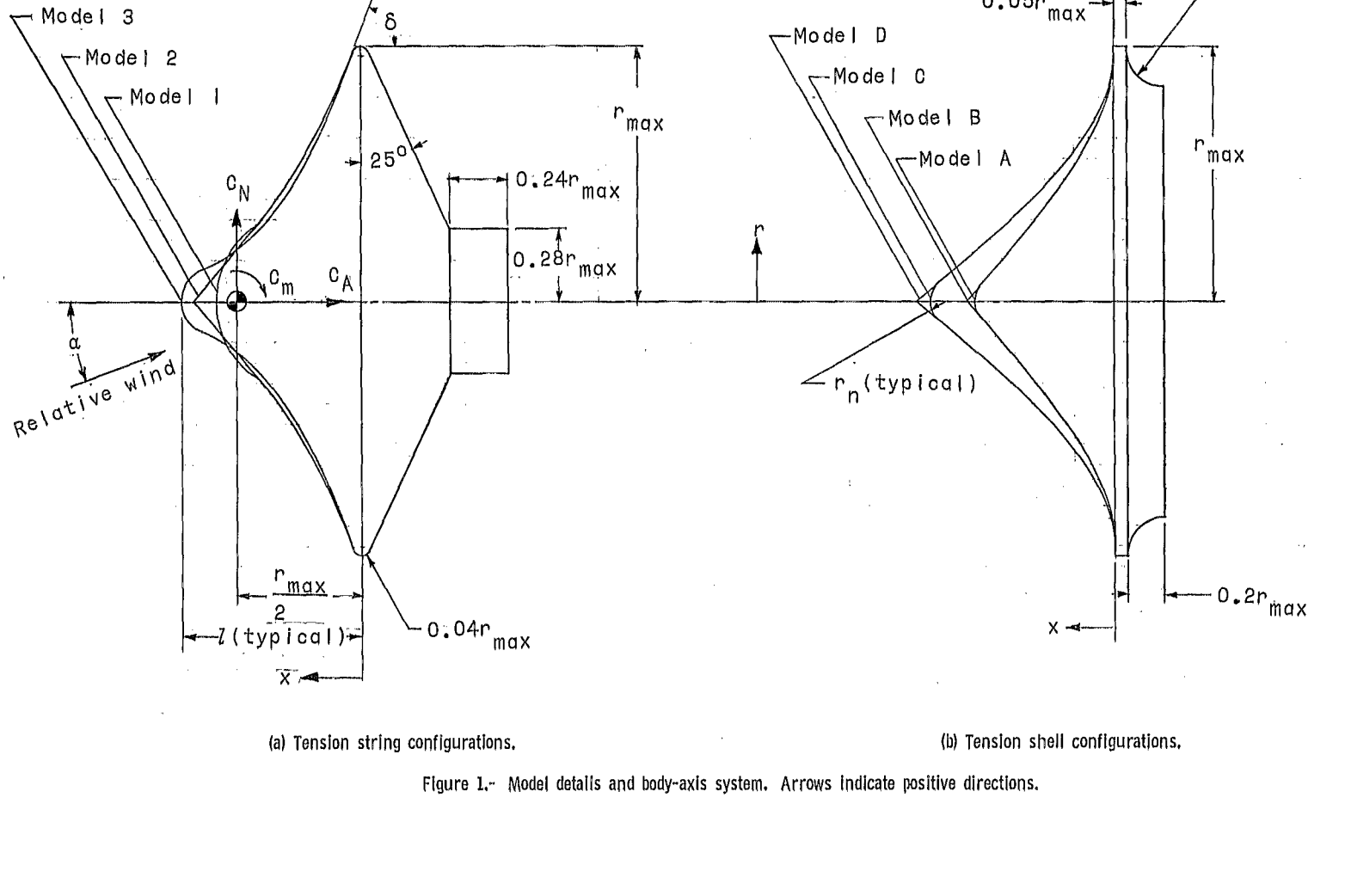

(a) Tension string configurations.

(b) Tension shell configurations.

Figure 1.- Model details and body-axis system. Arrows indicate positive directions.

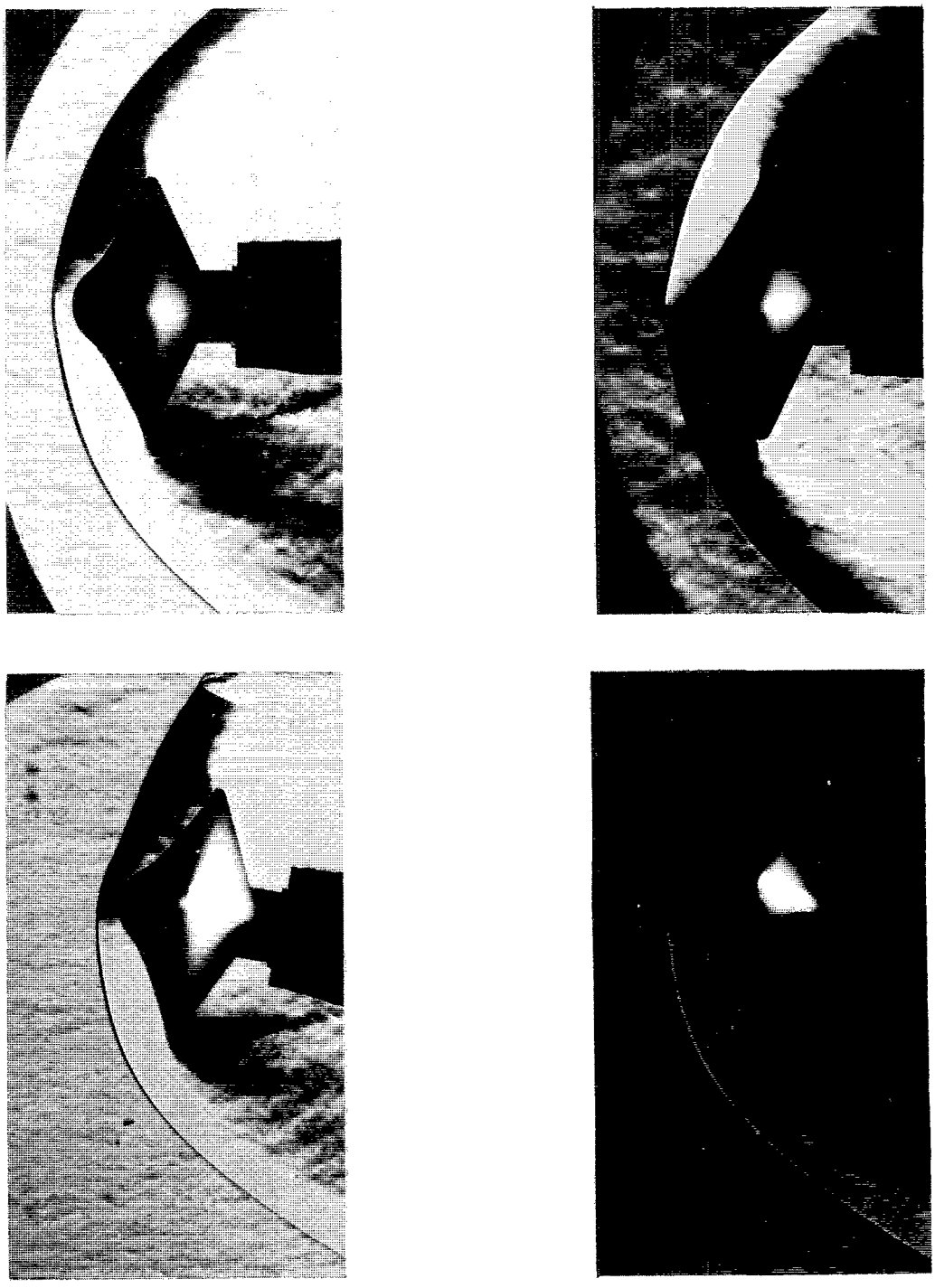

Figure 2.- Schlieren photographs of tension string shapes (models 1, 2, and 3), 120° cone, and tension shell shapes (models A, B, C, and D) at $R \approx 1.0 \times 10^6$. L-67-6691

$\alpha = 0°$

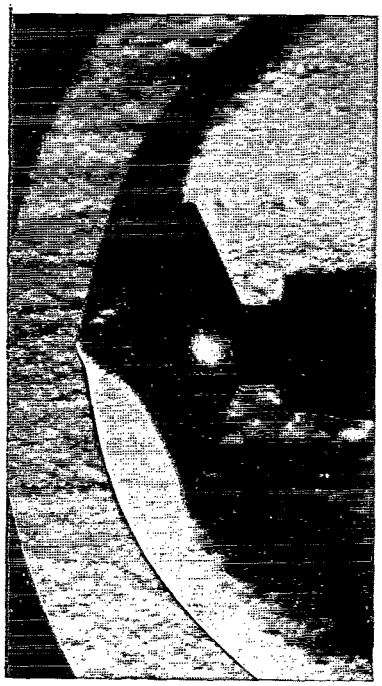

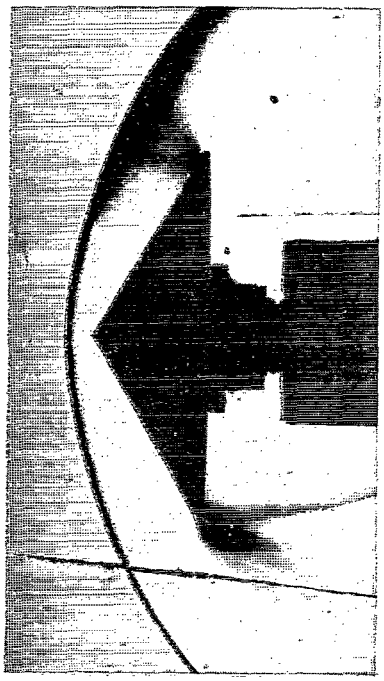

$\alpha = 12°$

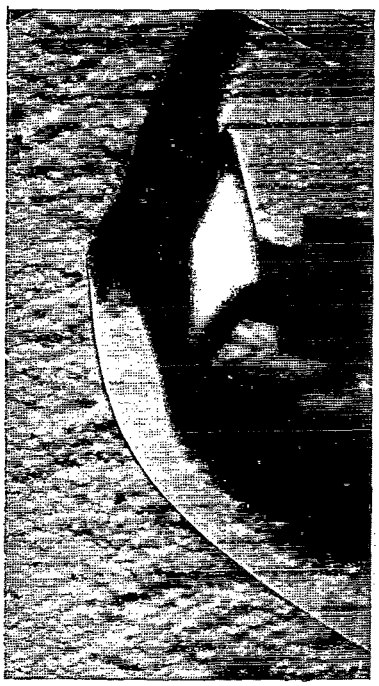

Model 3

120° cone

Figure 2.- Continued.

L-67-6692

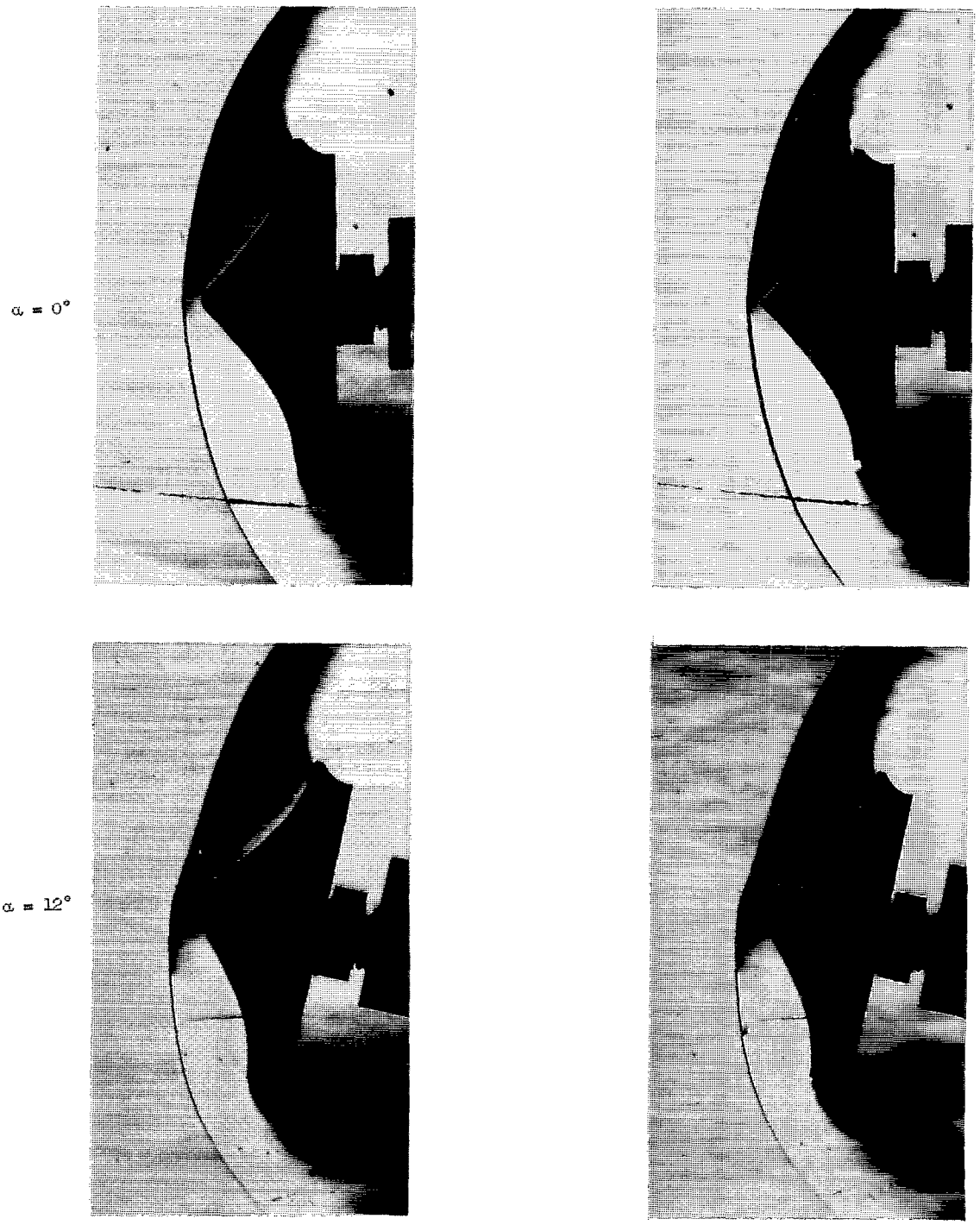

Figure 2.- Continued.

L-67-6693

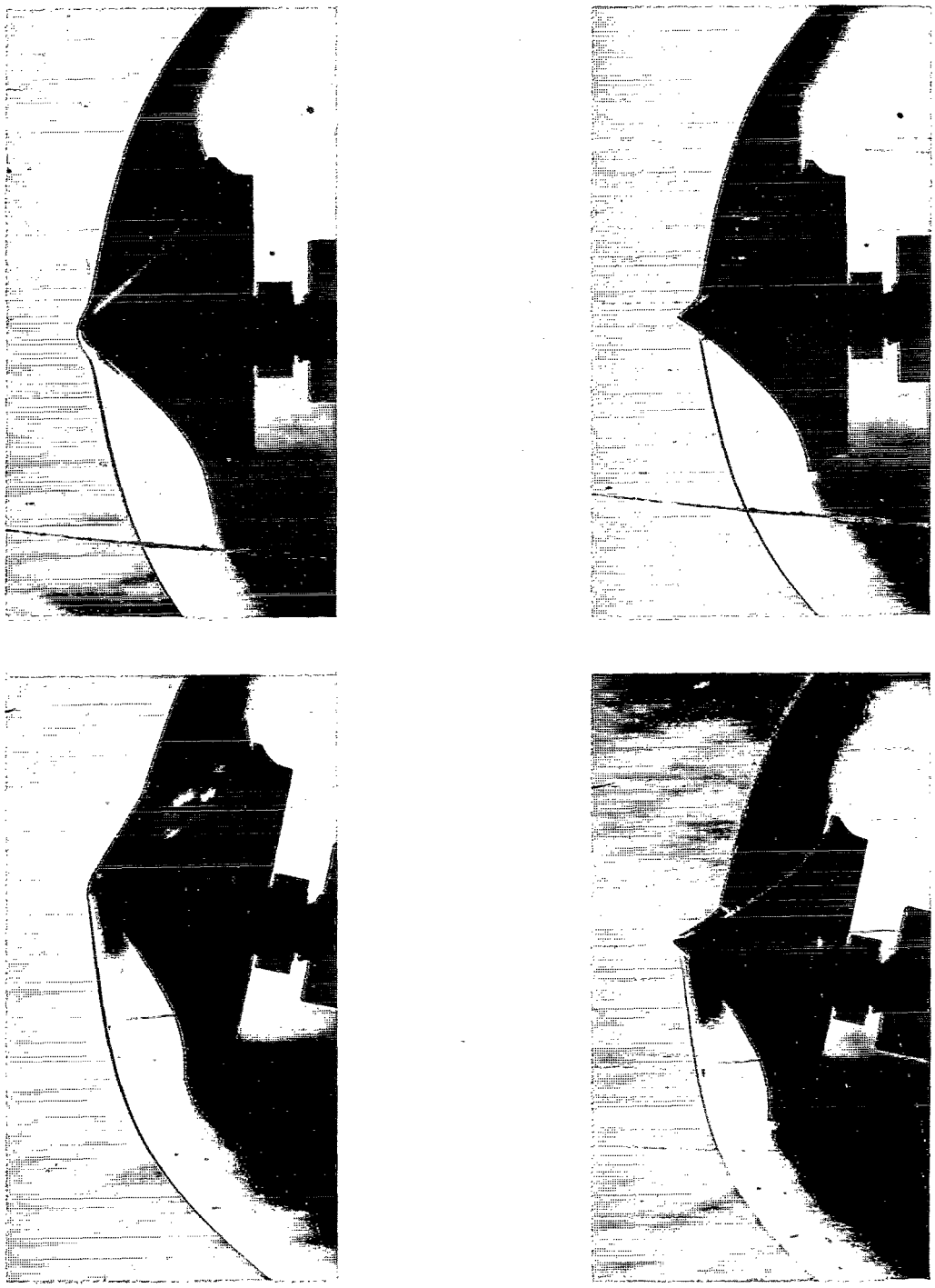

Figure 2.- Concluded.

L-67-6694

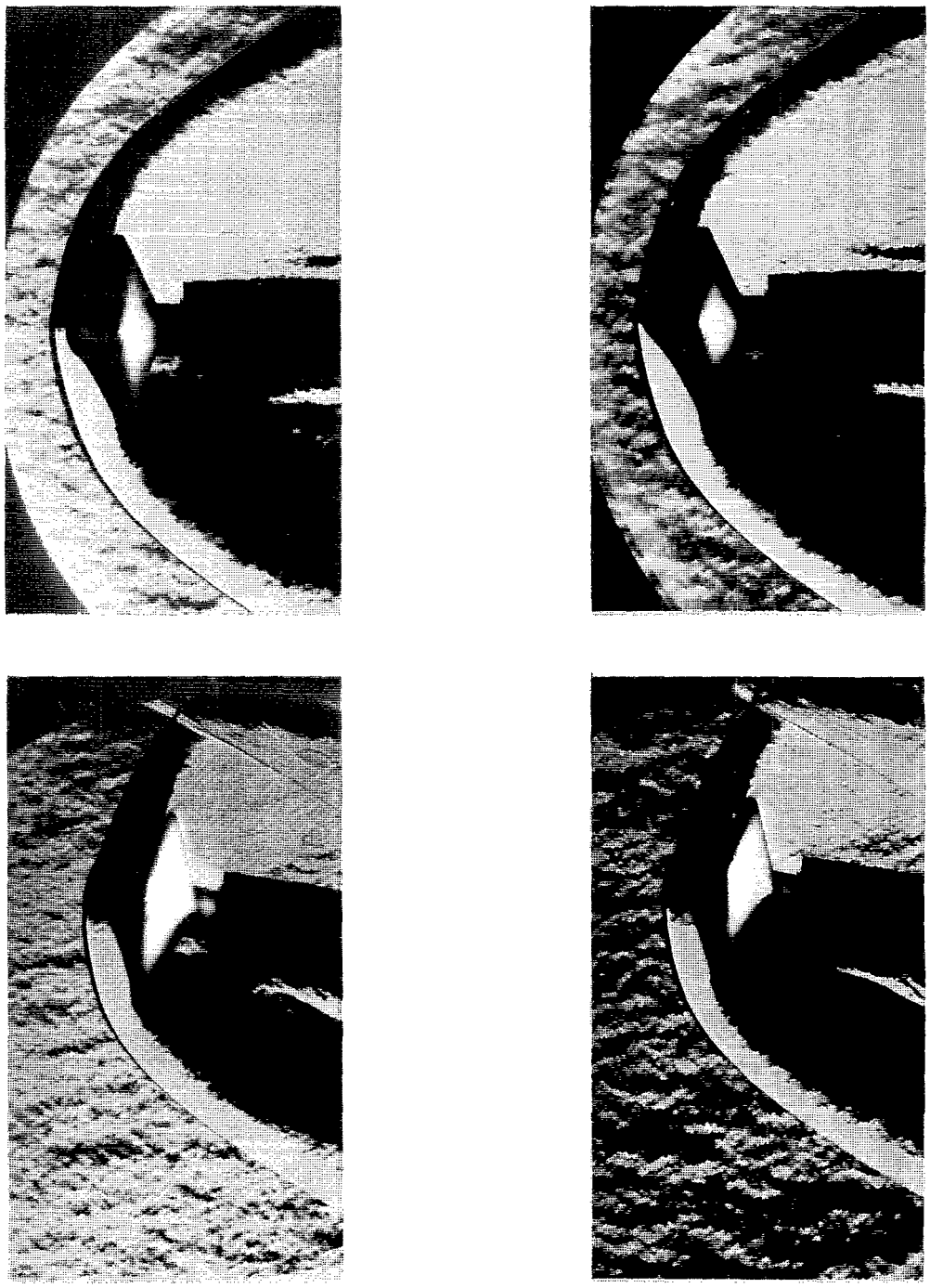

Figure 3.- Schlieren photographs of tension string shapes (models 1, 2, and 3), 120° cone, and tension shell shapes (models A, B, C, and D) at $R \approx 3.0 \times 10^6$. L-67-6695

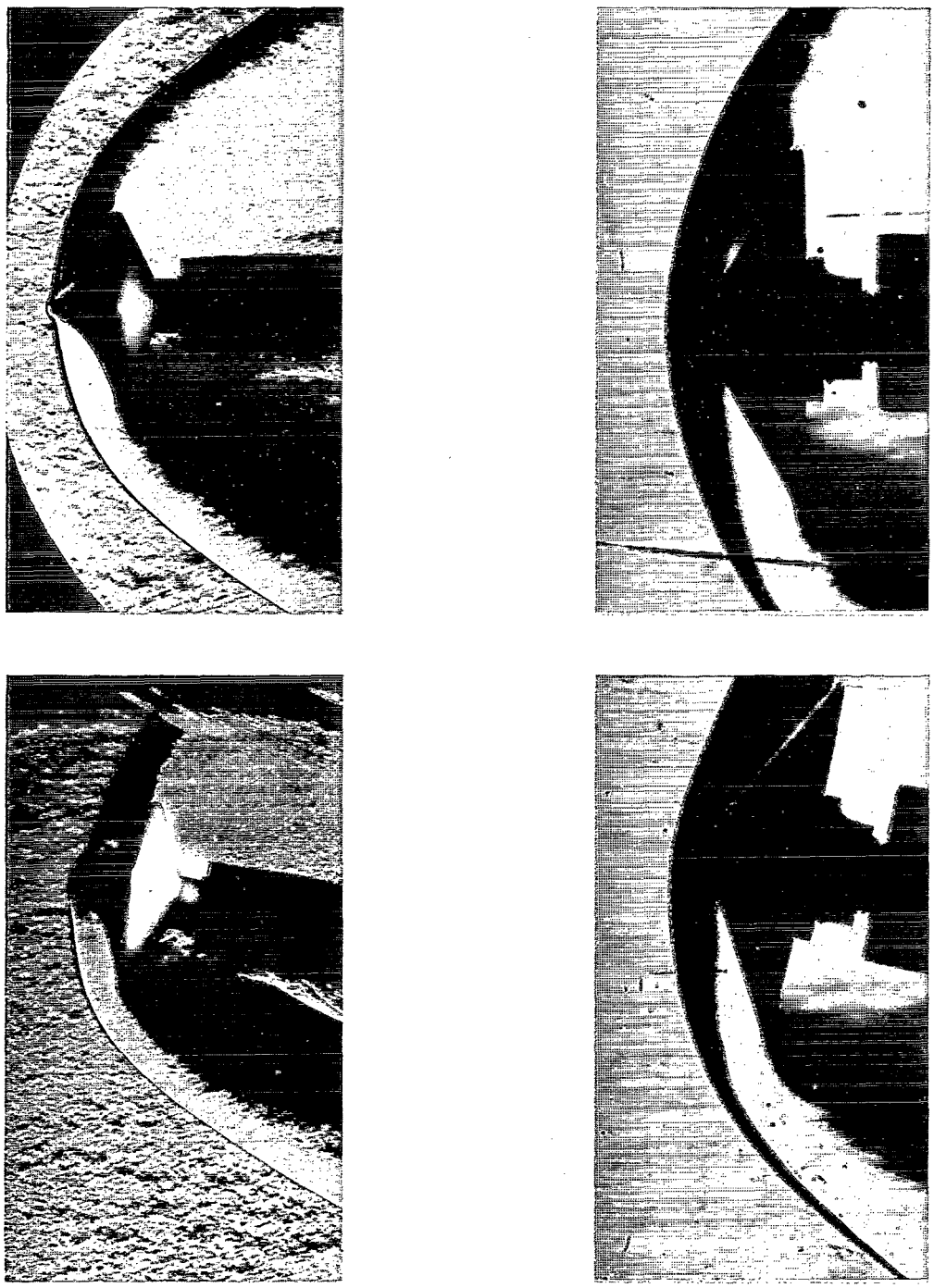

Figure 3.- Continued. L-67-6696

$\alpha = 0°$

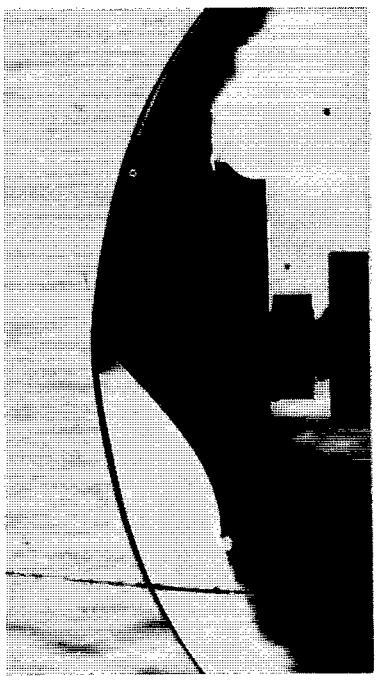

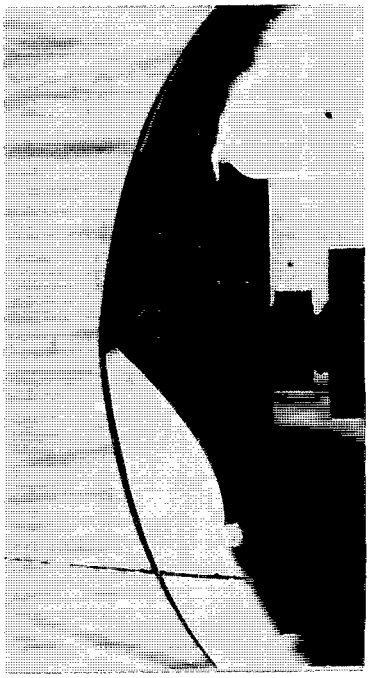

$\alpha = 12°$

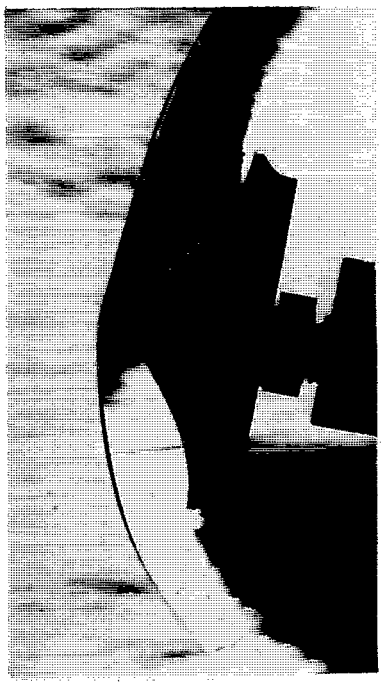

Model A

Model B

Figure 3.- Continued.

L-67-6697

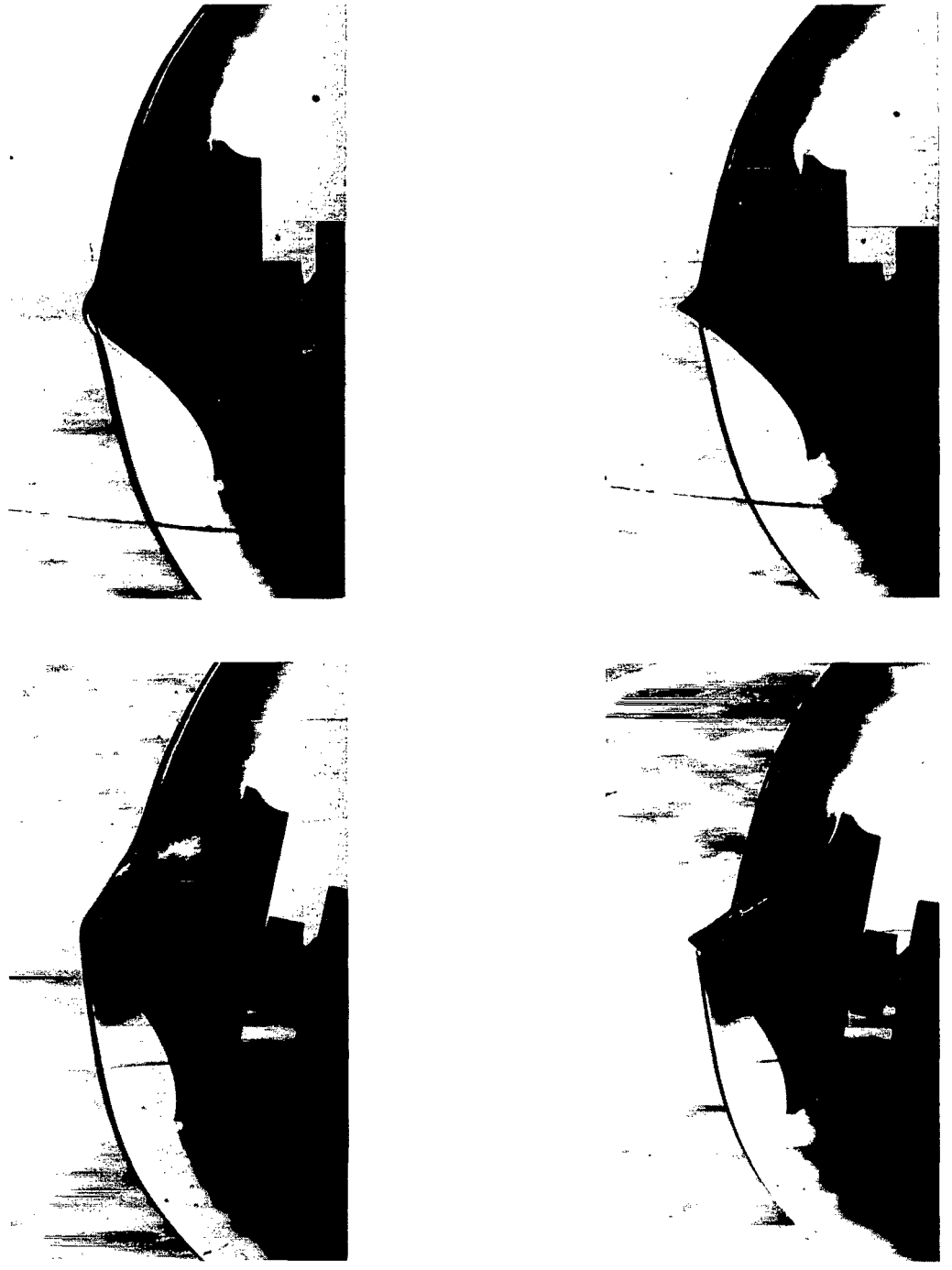

Figure 3.- Concluded. L-67-6698

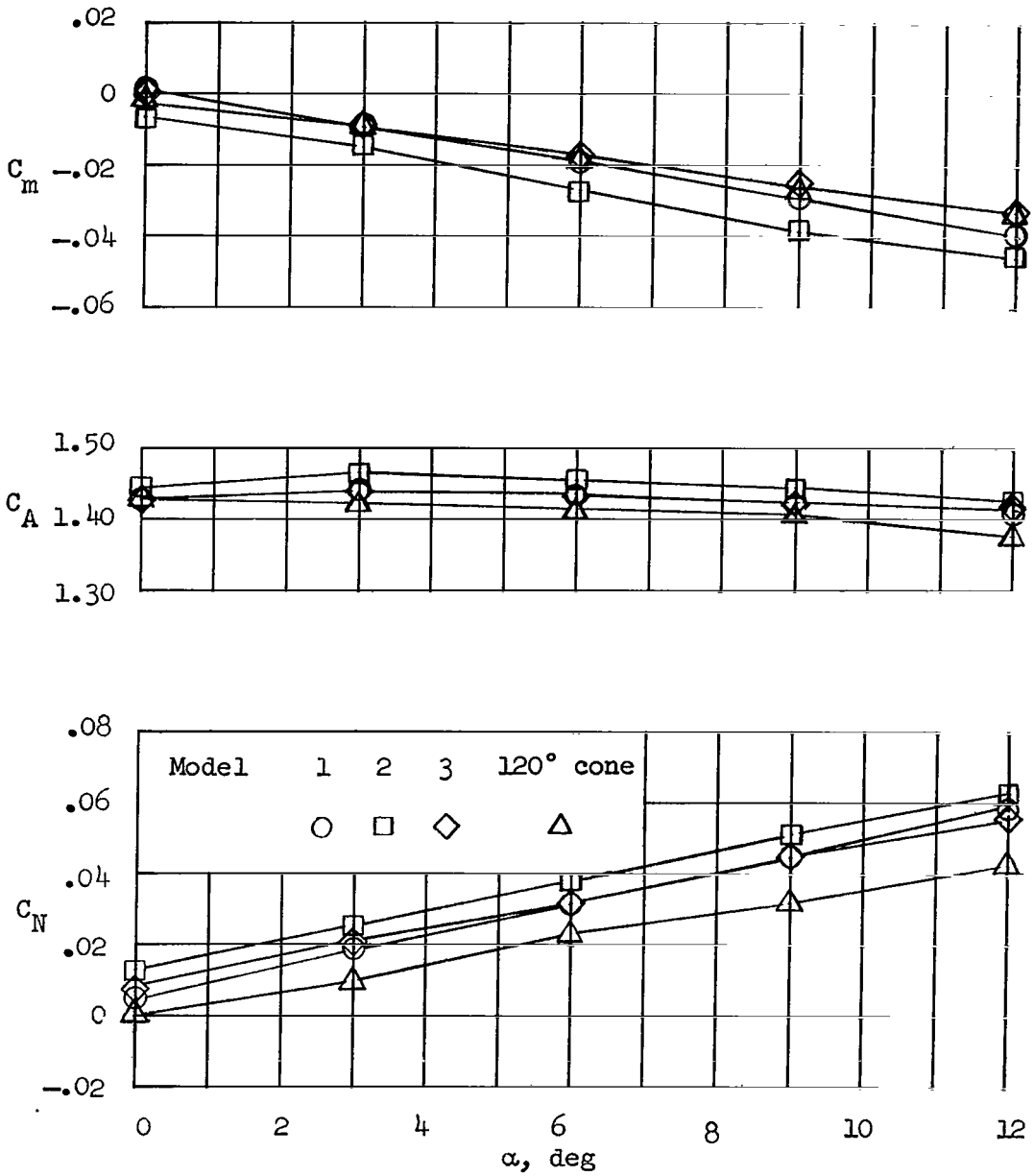

Figure 4.- Longitudinal aerodynamic characteristics of models at $R \approx 1.0 \times 10^6$.

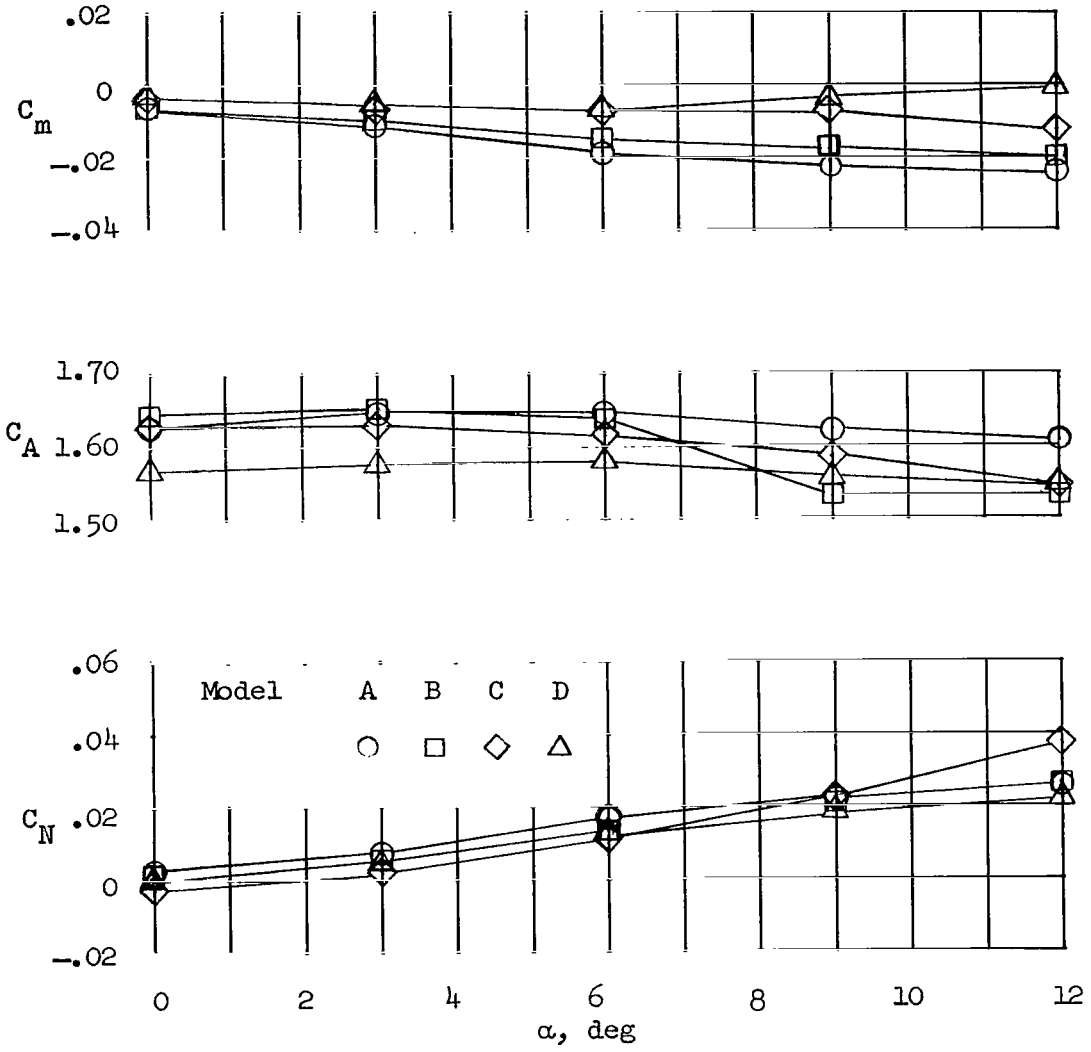

Figure 4.- Concluded.

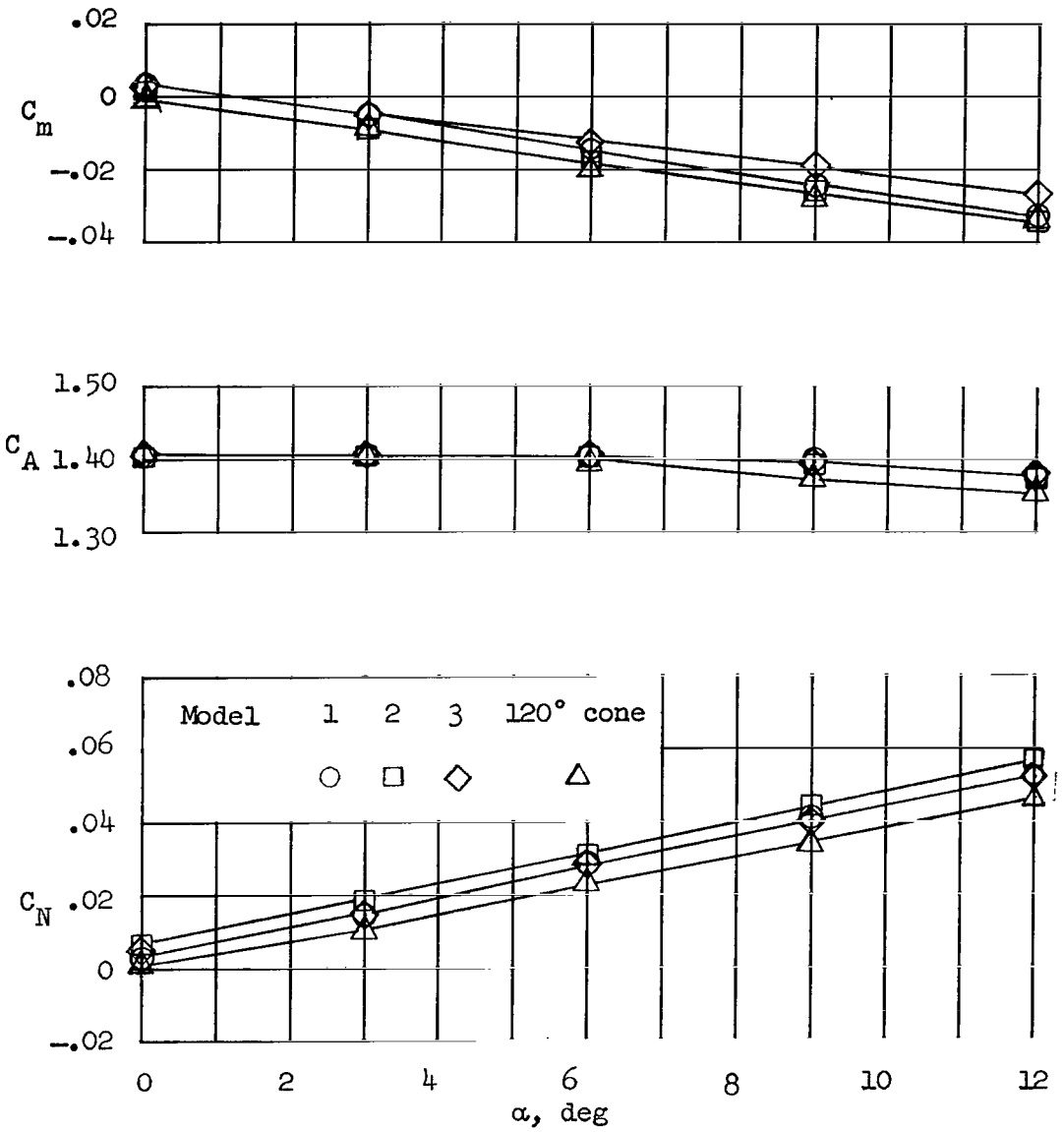

Figure 5.- Longitudinal aerodynamic characteristics of models at $R \approx 3.0 \times 10^6$.

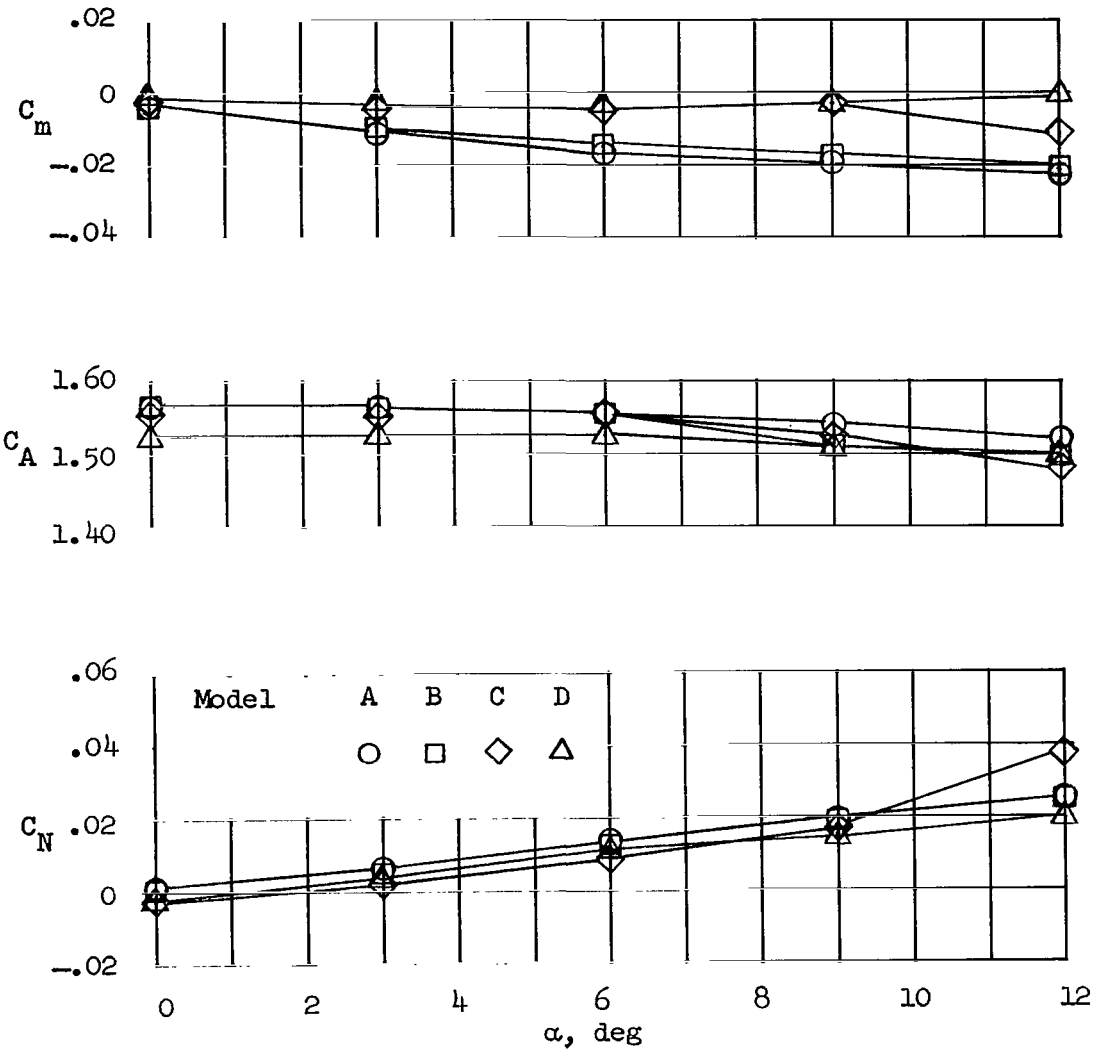

Figure 5.- Concluded.

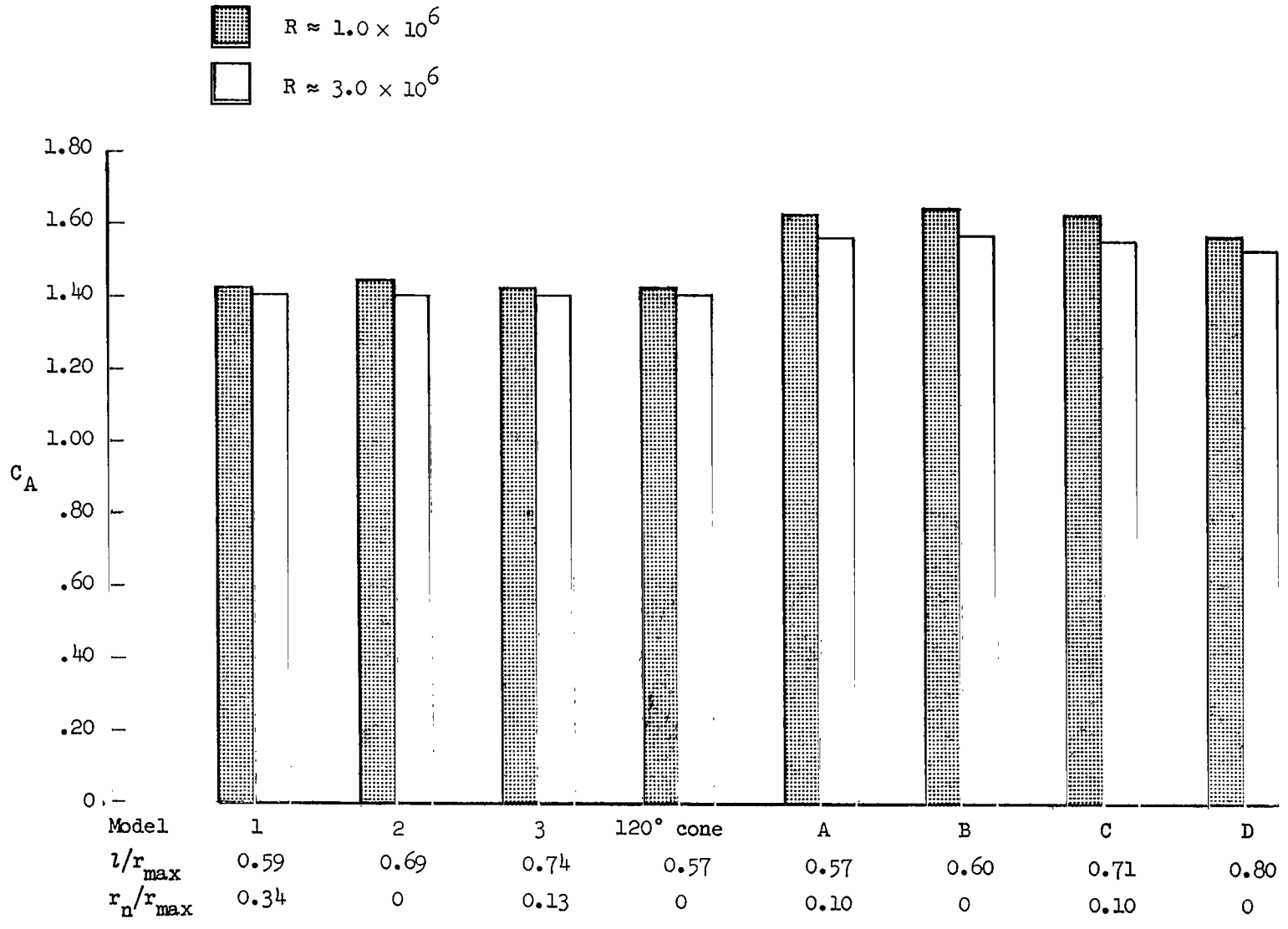

Figure 6.- Axial-force coefficients at $\alpha = 0^{\circ}$ for each model.

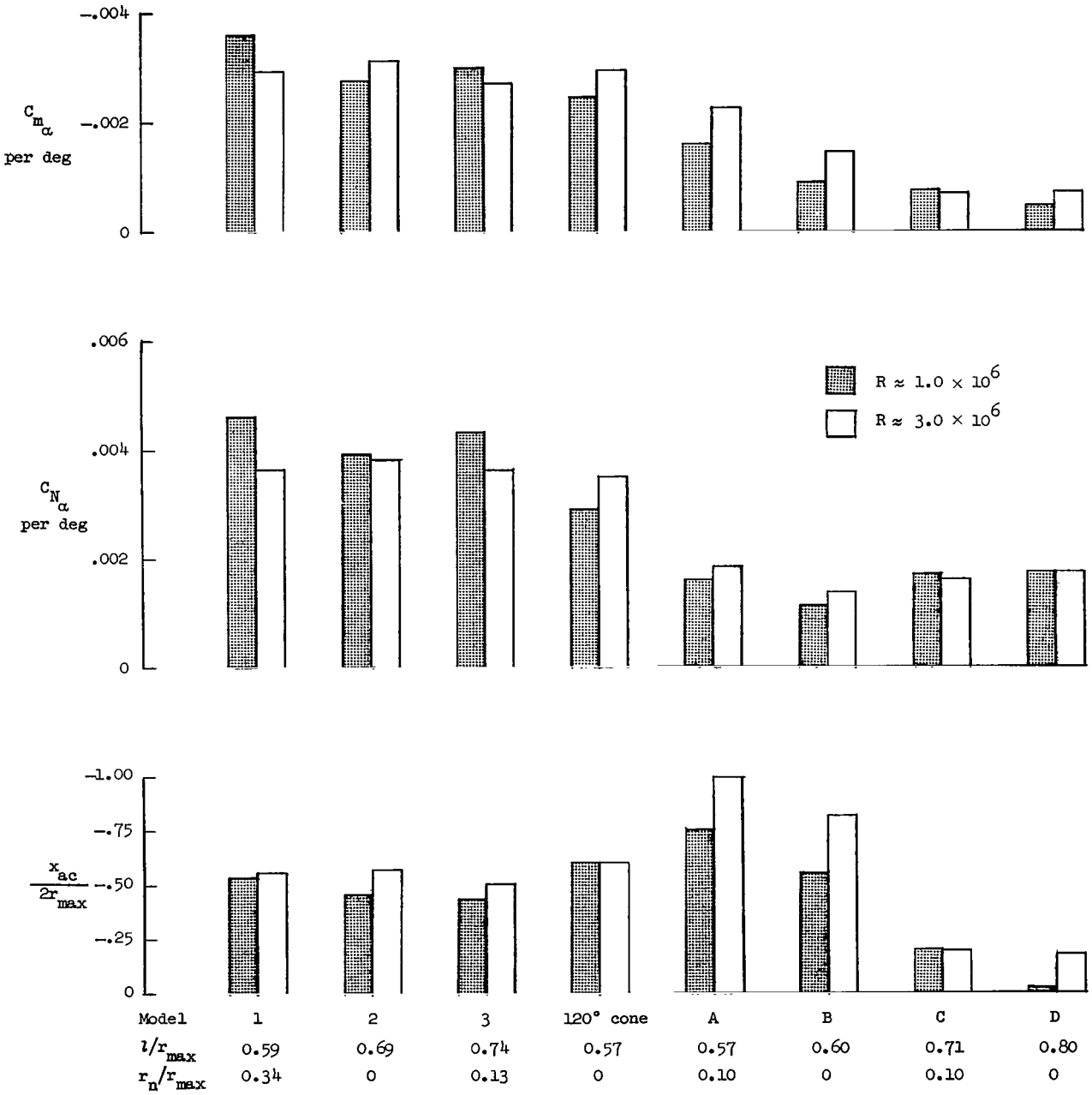

Figure 7.- C_{m_α}, C_{N_α}, and $x_{ac}/2r_{max}$ for each model.

"The aeronautical and space activities of the United States shall be conducted so as to contribute . . . to the expansion of human knowledge of phenomena in the atmosphere and space. The Administration shall provide for the widest practicable and appropriate dissemination of information concerning its activities and the results thereof."

—NATIONAL AERONAUTICS AND SPACE ACT OF 1958

NASA SCIENTIFIC AND TECHNICAL PUBLICATIONS

TECHNICAL REPORTS: Scientific and technical information considered important, complete, and a lasting contribution to existing knowledge.

TECHNICAL NOTES: Information less broad in scope but nevertheless of importance as a contribution to existing knowledge.

TECHNICAL MEMORANDUMS: Information receiving limited distribution because of preliminary data, security classification, or other reasons.

CONTRACTOR REPORTS: Scientific and technical information generated under a NASA contract or grant and considered an important contribution to existing knowledge.

TECHNICAL TRANSLATIONS: Information published in a foreign language considered to merit NASA distribution in English.

SPECIAL PUBLICATIONS: Information derived from or of value to NASA activities. Publications include conference proceedings, monographs, data compilations, handbooks, sourcebooks, and special bibliographies.

TECHNOLOGY UTILIZATION PUBLICATIONS: Information on technology used by NASA that may be of particular interest in commercial and other non-aerospace applications. Publications include Tech Briefs, Technology Utilization Reports and Notes, and Technology Surveys.

Details on the availability of these publications may be obtained from:

SCIENTIFIC AND TECHNICAL INFORMATION DIVISION

NATIONAL AERONAUTICS AND SPACE ADMINISTRATION

Washington, D.C. 20546